HEPATOLOGY

HEPATOLOGY, VOL. 73, NO. 6, 2021

LIVER BIOLOGY/PATHOBIOLOGY

Hexa Histidine–Tagged Recombinant Human Cytoglobin Deactivates Hepatic Stellate Cells and Inhibits Liver Fibrosis by Scavenging Reactive Oxygen Species

Ninh Quoc Dat,[1,2*] Le Thi Thanh Thuy,[1*] Vu Ngoc Hieu,[1] Hoang Hai,[1] Dinh Viet Hoang,[1] Nguyen Thi Thanh Hai,[3] Tuong Thi Van Thuy,[4] Tohru Komiya,[5] Krista Rombouts,[6] Minh Phuong Dong,[1] Ngo Vinh Hanh,[1] Truong Huu Hoang,[1] Misako Sato-Matsubara,[1] Atsuko Daikoku,[1] Chiho Kadono,[1] Daisuke Oikawa,[7] Katsutoshi Yoshizato,[8,9] Fuminori Tokunaga,[7] Massimo Pinzani,[6] and Norifumi Kawada[1,6]

BACKGROUND AND AIMS: Antifibrotic therapy remains an unmet medical need in human chronic liver disease. We report the antifibrotic properties of cytoglobin (CYGB), a respiratory protein expressed in hepatic stellate cells (HSCs), the main cell type involved in liver fibrosis.

APPROACH AND RESULTS: *Cygb*-deficient mice that had bile duct ligation–induced liver cholestasis or choline-deficient amino acid–defined diet–induced steatohepatitis significantly exacerbated liver damage, fibrosis, and reactive oxygen species (ROS) formation. All of these manifestations were attenuated in *Cygb*-overexpressing mice. We produced hexa histidine–tagged recombinant human CYGB (His-CYGB), traced its biodistribution, and assessed its function in HSCs or in mice with advanced liver cirrhosis using thioacetamide (TAA) or 3,5-di ethoxycarbonyl-1,4-dihydrocollidine (DDC). In cultured HSCs, extracellular His-CYGB was endocytosed and accumulated in endosomes through a clathrin-mediated pathway. His-CYGB significantly impeded ROS formation spontaneously or in the presence of ROS inducers in HSCs, thus leading to the attenuation of collagen type 1 alpha 1 production and α-smooth muscle actin expression. Replacement the iron center of the heme group with cobalt nullified the effect of His-CYGB. In addition, His-CYGB induced interferon-β secretion by HSCs that partly contributed to its antifibrotic function. Momelotinib incompletely reversed the effect of His-CYGB. Intravenously injected His-CYGB markedly suppressed liver inflammation, fibrosis, and oxidative cell damage in mice administered TAA or DDC mice without adverse effects. RNA-sequencing analysis revealed the down-regulation of inflammation- and fibrosis-related genes and the up-regulation of antioxidant genes in both cell culture and liver tissues. The injected His-CYGB predominantly localized to HSCs but not to macrophages, suggesting specific targeting effects. His-CYGB exhibited no toxicity in chimeric mice with humanized livers.

CONCLUSIONS: His-CYGB could have antifibrotic clinical applications for human chronic liver diseases. (Hepatology 2021;73:2527-2545).

Hepatic fibrosis is a common pathological process associated with chronic liver diseases that can result in the development of cirrhosis,

Abbreviations: 4-HNE, 4-hydroxynonenal; ALT, alanine aminotransferase; AST, aspartate aminotransferase; BDL, bile duct ligation; CD31, cluster of differentiation 31; CD68, cluster of differentiation 68; CDAA, choline-deficient amino acid–defined; Co-CYGB, cobalt CYGB; COL1A1, collagen type 1 alpha 1; Cont, untreated control; CYGB, cytoglobin; Cygb-mCherry, Cygb with mCherry reporter overexpression; Cyp, cytochrome P450; DCFDA, 2',7'-dichlorofluorescein diacetate; DDC, 3,5-diethoxycarbonyl-1,4-dihydrocollidine; GSH, reduced glutathione; GSSG, oxidized glutathione; H&E, hematoxylin and eosin; HC, hepatocyte; HHSteC, human HSC; His-CYGB, 6His-tagged rhCYGB; HSC, hepatic stellate cell; HX, hypoxanthine; XO, xanthine oxidase; IFI, IFN-inducible; IFN, interferon; IHC, immunohistochemistry; IRF, IFN regulatory factor; JAK, Janus kinase; LDH, lactate dehydrogenase; mHC, mouse HC; mHSC, mouse HSC; MMP, matrix metalloproteinase; $O2^{\bullet-}$, superoxide anion radical; $OH^{\bullet}$, hydroxyl radical; P-, phosphorylated; PXB mice, chimeric mice with humanized livers; qRT-PCR, quantitative RT-PCR; rh, recombinant human; RNA-Seq, RNA sequencing; ROS, reactive oxygen species; SiR-FG, Sirius red and fast green; SOD, superoxide dismutase; STAT, signal transducer and activator of transcription; TAA, thioacetamide; TAC, total antioxidant capacity; TAT, trans-activator of transcription; TAT-CYGB, TAT-tagged rhCYGB; TBA, total bile acid; TBK1, TANK-binding kinase 1; TEM, transmission electron microscopy; TGF-β, transforming growth factor-β; Timp-1, tissue inhibitor of metalloproteinase 1; TUNEL, terminal deoxynucleotide transferase dUTP nick end-labeling; WT, wild type; αSMA, α-smooth muscle actin.

Received December 2, 2020; accepted January 6, 2021.

liver failure, and hepatocellular carcinoma (HCC).[1] Regardless of their etiology, liver fibrotic processes are mediated by interactions and cross-talk between hepatic cells and infiltrating inflammatory cells and modulated by the release of several mediators, including growth factors, cytokines, chemokines, adipokines, vasoactive compounds, and reactive oxygen species (ROS).[2] The involvement of ROS in liver fibrosis was first described in 1965, by Comporti et al.[3] and Ghoshal et al.[4], who reported the induction of liver injury by CCl_4 through lipid peroxidation. Oxidative stress is known to be involved in liver trauma and fibrosis, triggered by ethanol intake[5], NASH[6], iron overload[7], and HCV infection.[8] Fibrogenic progression during these diseases has been associated with significantly decreased and/or impaired antioxidant defenses, such as copper/zinc–superoxide dismutase (SOD)[9] and manganese-SOD (Mn-SOD).[10]

Hepatic stellate cells (HSCs), which are the primary cell type involved in liver fibrosis, are activated by exposure to cytokines and ROS derived from damaged hepatocytes (HCs), activated Kupffer cells, sinusoidal endothelial cells, or other HSCs through autocrine or paracrine signaling mechanisms.[11] ROS generated by infiltrating neutrophils and macrophages can also activate HSCs.[12] Although most HCs contain large ROS-scavenging enzymatic systems, including catalase in peroxisomes and Mn-SOD in mitochondria, HSCs are the only liver cell type that expresses cytoglobin (CYGB),[13] a member of the mammalian globin family, which has a ROS-scavenging function.[14,15]

CYGB exhibits intrinsic O_2-binding capacities because its heme iron has the same affinities for exogenous ligands and the same oxygen equilibrium constants as myoglobin.[13] *In vivo*, CYGB deficiency causes severe oxidative stress and the spontaneous induction of HCC in mice,[16,17] whereas the selective overexpression of CYGB can prevent the H_2O_2-induced activation of HSCs.[18] Thus, CYGB may act as an elite gatekeeper, protecting HSCs from ROS-induced damage or activation.

Recently, evidence has suggested that the interferon-β (IFN-β) signaling pathway, through the activation of the Janus kinase (JAK)/signal transducer and activator of transcription (STAT) pathway, may play a key role in controlling liver fibrosis.[19] IFN-β treatment reduces concanavalin A–induced hepatic fibrosis by inhibiting the mRNA expression of transforming

Additional Supporting Information may be found at onlinelibrary.wiley.com/doi/10.1002/hep.31752/suppinfo.

**These authors shared co-first authorship.*

Supported by the Japanese Government Scholarship for the Ph.D. course (to N.Q.D.), a grant-in-aid for scientific research from the Japan Society for the Promotion of Science (JSPS) (J192640023; to L.T.T.T.), the Gilead Science for Research Scholars Program in Liver Diseases (FY2019-202J1; to L.T.T.T.), a grant-in-aid for scientific research from the JSPS (J192640002 to N.K.), and a Research Program on Hepatitis grant from the Japan Agency for Medical Research and Development (AMED-J202620103 to N.K.).

View this article online at wileyonlinelibrary.com.

DOI 10.1002/hep.31752

Potential conflict of interest: Nothing to report.

ARTICLE INFORMATION:

From the [1]Department of Hepatology, Graduate School of Medicine, Osaka City University, Osaka, Japan; [2]Department of Pediatrics, Hanoi Medical University, Hanoi, Vietnam; [3]Department of Biochemistry, Hanoi Medical University, Hanoi, Vietnam; [4]Biological Resources Vinmec Tissue Bank, Vinmec Healthcare System, Hanoi, Vietnam; [5]Department of Biology, Faculty of Science, Osaka City University, Osaka, Japan; [6]Regenerative Medicine and Fibrosis Group, Institute for Liver and Digestive Health, University College London, Royal Free Hospital, London, United Kingdom; [7]Department of Pathobiochemistry, Graduate School of Medicine, Osaka City University, Osaka, Japan; [8]Academic Advisor's Office, PhoenixBio Co., Ltd., Hiroshima, Japan; [9]Endowed Laboratory of Synthetic Biology, Graduate School of Medicine, Osaka City University, Osaka, Japan.

ADDRESS CORRESPONDENCE AND REPRINT REQUESTS TO:

Norifumi Kawada, M.D., Ph.D.
Department of Hepatology, Graduate School of Medicine
Osaka City University
1-4-3 Asahimachi, Abeno, Osaka 545-8585, Japan
E-mail: kawadanori@med.osaka-cu.ac.jp
Tel.: +81-6-6645-3897

growth factor-β (TGF-β), basic fibroblast growth factor, collagen type 1 alpha 2 (*Col1a2*), and tissue inhibitor of metalloproteinase 1 (*Timp-1*).[20]

Herein, we report the following antifibrotic properties of CYGB. First, bile duct ligation (BDL) and steatohepatitis models induced in *Cygb*-deficient mice displayed exacerbated liver damage, fibrosis, and ROS formation, which were attenuated in mice with *Cygb* with mCherry reporter overexpression (*Cygb-mCherry*). Second, we demonstrated spontaneous endocytosis and endosomal accumulation of exogenous hexa histidine (6His)-tagged recombinant human (rh) CYGB (His-CYGB) in HSCs, resulting in the suppression of HSC activation–associated manifestations through ROS-scavenging functions. In addition, exogenous His-CYGB induced IFN-β secretion from HSCs by activating TRAF Family Member Associated NFKB Activator-binding kinase 1 (TBK1), resulting in the induction of the JAK/STAT pathway. Third, we found that intravenously injected His-CYGB was delivered to HSCs in mice and contributed to the prevention of fibrosis progression induced by thioacetamide (TAA) or 3,5-diethoxycarbonyl-1,4-dihydrocollidine (DDC) administration. Fourth, His-CYGB intravenously injected into chimeric mice with humanized livers (PXB mice) exhibited no toxicity. Combined, our data support the potential application of His-CYGB as an antifibrotic therapy in humans.

Materials and Methods

rhCYGB PRODUCTION

The open reading frame of cloned human CYGB complementary DNA fused with 6His or transactivator of transcription (TAT) tags was expressed in *Escherichia coli* BL-21AI cells. rhCYGB was purified by immobilized metal ion affinity chromatography (HisTALON superflow; Takara Bio), polished by size exclusion chromatography (HiLoad 16/600 Superdex, 75 pg; GE Healthcare), and concentrated with Amicon Ultra-1 (Merck Millipore Ltd., Co.). In total, three kinds of rhCYGB were produced in our laboratory, including His-CYGB, TAT-tagged rhCYGB (TAT-CYGB) and cobalt CYGB (Co-CYGB).

MICE

Cygb-deficient and *Cygb-mCherry* mice (Supporting Fig. S1) were generated in our laboratory as described.[18,21] Briefly, in *Cygb-mCherry* mice, exogenous *Cygb* was incorporated with a *2A-mCherry* tag under the regulation of the *Cygb* promoter, which directs gene expression in target *Cygb*-expressing cells. In the liver, Cygb is overexpressed only in HSCs. The founder *Cygb-mCherry* mice were backcrossed with C57BL/6J wild-type (WT) mice for 3-6 generations, and only their offspring with 10 *Cygb* copies were used in this study. C57BL/6J WT mice were purchased from Japan SLC Inc. WT mice were cohoused with *Cygb*-deficient mice and *Cygb-mCherry* mice for at least 1 week before experiments. PXB mice showing a replacement index of more than 90% were purchased from PhoenixBio Co., Ltd.

All mice received humane care, according to Guide for the Care and Use of Laboratory Animals, National Institutes of Health. All protocols and experimental procedures were approved by the Institutional Animal Care and Use Committee of Osaka City University and were performed following the guidelines of the National Institutes of Health for the use of animals in research. See the Supporting Information for details of mouse BDL studies; choline-deficient amino acid–defined (CDAA) diet administration; and His-CYGB treatment in normal WT mice, PXB mice, TAA-treated mice, or DDC diet–fed mice.

CELL CULTURE AND TREATMENT

Human HSCs (HHSteCs) were purchased from ScienCell Research Laboratories. Primary human HSCs (hHSCs) were obtained from the Institute for Liver and Digestive Health, Royal Free Hospital, University College London (NC2015.020 [B-ERC-RF]). Primary mouse HSCs (mHSCs) and primary mouse HCs (mHCs) were isolated from WT mice in our laboratory as described.[18] See the Supporting Information for details.

IN VITRO AND *IN VIVO* DISTRIBUTION OF HIS-CYGB

The translocation and distribution of His-CYGB were determined using His-CYGB unlabeled and labeled with Alexa tetrafluorophenyl (TFP) esters, which were obtained from Molecular Probes and included Alexa Fluor 488 and Alexa Fluor 647. TFP

esters react efficiently with the primary amines in proteins to form stable dye–protein conjugates. Proteins were labeled following the manufacturer's protocol. For transmission electron microscopy (TEM) (Talos F200X S/TEM; Thermo Fisher Scientific) analysis, His-CYGB was performed after embedding labeling using 5-nm nickel–nitrilotriacetic (Ni-NTA) nanogold particles (Nanoprobes). See the Supporting Information for details.

RNA SEQUENCING AND DATA ANALYSIS

RNA sequencing (RNA-seq) was performed on HHSteCs and TAA/DDC-treated liver tissues, with or without His-CYGB treatment (n = 3 each group). Total RNA was extracted and used for the library preparation process. RNA libraries were then sequenced using the NovaSeq 6000 platform (Macrogen). RNA-seq data have been deposited in the Gene Expression Omnibus database and can be accessed using the identifier GSE156780. See the Supporting Information for details.

STATISTICAL ANALYSIS

All experiments were replicated at least three times. ImageJ was used to evaluate the band intensities for immunoblotting analysis (National Institutes of Health). The data presented as bar graphs are the means ± standard deviations for all experiments. Statistical analyses were performed using a Student *t* test (two-tailed) or ANOVA followed by Tukey multiple comparison tests. Significant differences among groups are indicated as $^{*}P < 0.05$, $^{**}P < 0.01$, and $^{***}P < 0.001$. Calculations were performed using GraphPad Prism 8.0 (GraphPad Software, Inc.).

All information about the materials and methods is available in the Supporting Information.

Results

CYGB REGULATES LIVER INJURY, INFLAMMATION, AND FIBROSIS IN MICE

We reported the down-regulation of CYGB expression in HHSteCs sourced from the livers of patients with HCV-induced fibrosis[22] and compared the development of liver fibrosis and cancer between liver injury models generated in *Cygb*-deficient mice and WT mice.[16,17,21,23] To gain further insights into the role of CYGB during liver trauma, *Cygb-mCherry* mice were generated and used in two different liver injury models: BDL-induced cholestasis (Fig. 1) and CDAA-induced steatohepatitis (Supporting Fig. S2). Compared with WT control mice, during the acute phase of BDL (48 hours), *Cygb*-deficient mice presented the following:

1. More numerous bile infarcts and increased terminal deoxynucleotide transferase deoxyuridine triphosphate nick end-labeling (TUNEL)-positive HC deaths (Fig. 1A);
2. Higher serum levels of aspartate aminotransferase (AST), alanine aminotransferase (ALT), total bilirubin, and hepatic total bile acid (TBA) (Fig. 1B);
3. Increased accumulation of neutrophils and cluster of differentiation 68 (CD68)-positive macrophages in the hepatic parenchyma (Fig. 1A);
4. Higher levels of chemokine (C-X-C motif) ligand 2 (*Cxcl-2)* and *Cxcl-5* mRNA expression (Fig. 1C);
5. Elevated levels of 4-hydroxynonenal (4-HNE); and
6. Decreased levels of the antioxidant nuclear factor erythroid 2–related factor 2 (NRF-2) (Fig. 1A).

These manifestations observed in *Cygb*-deficient mice were attenuated in *Cygb-mCherry* mice (Fig. 1A–C). During the chronic phase (1 and 2 weeks), liver tissue damage, TUNEL-positive HC death, inflammatory cell infiltration, and fibrotic events (collagen deposition, α-smooth muscle actin [αSMA]-positive HSC activation, collagen type 1 alpha 1 (*Col1a1*) mRNA expression, and 4-HNE expression) became aggravated in *Cygb*-deficient mice and were attenuated in *Cygb-mCherry* mice when compared with WT mice (Fig. 1D–F). Pro-oxidant transcripts, such as NADP oxidase 1 (*Nox-1*) and myeloperoxidase (*Mpo*), were up- and down-regulated in livers of *Cygb*-deficient and *Cygb-mCherry* mice, respectively, whereas antioxidative genes, including antioxidant 1 (*Atx-1*) and *N*-acetyltransferase 8 (*Nat-8*), showed the opposite effects (Fig. 1F).

Next, the mice were challenged with a CDAA diet for 16 weeks and allowed to recover for 4 weeks (Supporting Fig. S2). After 16 weeks of the CDAA diet, hepatic steatosis and liver fibrosis were

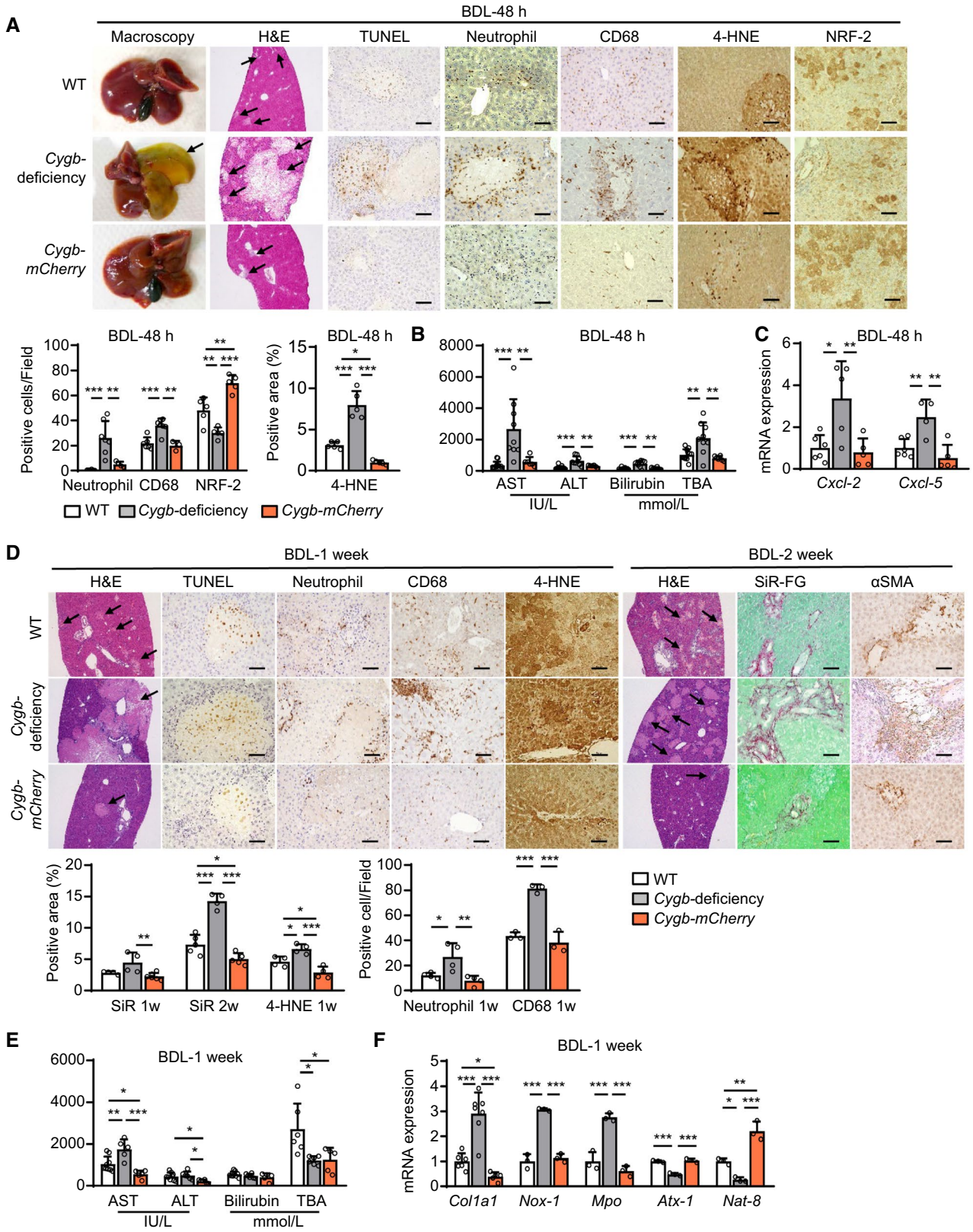
A
BDL-48 h
Macroscopy
H&E
TUNEL
Neutrophil
CD68
4-HNE
NRF-2
WT
Cygb-deficiency
Cygb-mCherry
BDL-48 h
Positive cells/Field
Neutrophil
CD68
NRF-2
Positive area (%)
4-HNE
B
BDL-48 h
AST
ALT
Bilirubin
TBA
IU/L
mmol/L
C
BDL-48 h
mRNA expression
Cxcl-2
Cxcl-5
WT
Cygb-deficiency
Cygb-mCherry
D
BDL-1 week
BDL-2 week
H&E
TUNEL
Neutrophil
CD68
4-HNE
H&E
SiR-FG
αSMA
WT
Cygb-deficiency
Cygb-mCherry
Positive area (%)
SiR 1w
SiR 2w
4-HNE 1w
Positive cell/Field
Neutrophil 1w
CD68 1w
WT
Cygb-deficiency
Cygb-mCherry
E
BDL-1 week
AST
ALT
Bilirubin
TBA
IU/L
mmol/L
F
BDL-1 week
mRNA expression
Col1a1
Nox-1
Mpo
Atx-1
Nat-8

FIG. 1. CYGB regulates BDL-induced cholestasis. (A-C) Severe liver injury and inflammation in *Cygb*-deficient mice and the reversal of liver injury in *Cygb-mCherry* mice under BDL at 48 hours (n = 6-12). (A) Representative liver macroscopic and microscopic images of H&E, TUNEL, and IHC staining for neutrophils, CD68 (macrophage marker), 4-HNE, and NRF-2 and their quantifications. (B) Serum levels of AST, ALT, bilirubin, and TBA as in A (n = 6-12). (C) qRT-PCR analysis of the liver as in A (n = 5-6). (D-F) Severe liver injury, inflammation, and fibrosis in *Cygb*-deficient mice and the reversal of injury in *Cygb-mCherry* mice under BDL at 1-2 weeks (n = 6-9). (D) Representative liver images of H&E, SiR-FG, TUNEL, and IHC staining for neutrophils, CD68, 4-HNE, and αSMA and their quantifications. (E) Serum level of AST, ALT, bilirubin, and TBA as in D (n = 6-9). (F) qRT-PCR analysis of the liver as in D (n = 3-7). $^{*}P < 0.05$, $^{**}P < 0.01$, and $^{***}P < 0.001$, one-way ANOVA followed by Tukey's multiple comparison tests. Arrows indicate bile infarcts. Scale bars, 50 μm. Abbreviations: H&E, hematoxylin and eosin; IHC, immunohistochemistry.

aggravated in *Cygb*-deficient mice and attenuated in *Cygb-mCherry* mice when compared with WT control mice (Supporting Fig. S2A, C, D). After 4 weeks of a normal diet, recovery was induced, with the exception of fibrosis in the livers of *Cygb*-deficient mice (Supporting Fig. S2B-D). Taken together, these observations from the BDL and CDAA models suggested that CYGB expression in HSCs provides a protective environment against liver inflammation and fibrosis in mice.

PRODUCTION OF HIS-CYGB AND ITS DISTRIBUTION *IN VITRO*

To test the hypothesis that CYGB exerts protective effects against liver damage, we generated high-purity His-CYGB (Supporting Fig. S3A). It displayed no toxicity against HHSteCs, showed no endotoxin contamination (Supporting Fig. S3B, C), and typically reduced and oxidized pyridine hemochromogen, based on spectrum measurements (Supporting Fig. S3D).

Surprisingly, when added to the culture medium, His-CYGB spontaneously attached to activated HHSteCs (Fig. 2A). Intracellular His-CYGB levels became elevated in a time- and dose-dependent manner (Fig. 2B). After HHSteCs were treated with His-CYGB (40 μg/mL) for 48 hours, the level of translocated His-CYGB (22.5 kDa) was 17.6-fold higher than that of endogenous CYGB (21 kDa) (Supporting Fig. S3E). His-CYGB localized to cytoplasmic, membrane, and cytoskeletal fractions but not to nuclear and chromatin-bound fractions (Fig. 2C). Alexa 488– and Alexa 647–labeled His-CYGB revealed its specific localization in the cytoplasm of HHSteCs (Fig. 2D and Supporting Fig. S3F) and also mHSCs (Supporting Fig. S4A). Partial colocalization of His-CYGB with the mitochondria and early and late endosomes and lysosomes (Fig. 2E), but not with the endoplasmic reticulum (Supporting Fig. S4B), were observed using corresponding organelle markers, indicating that His-CYGB enters the cells through endocytosis. Chlorpromazine (CPZ), a clathrin inhibitor, attenuated the incorporation of His-CYGB into HHSteCs more efficiently than nystatin, a caveolin inhibitor, or amiloride, a macropinocytosis inhibitor (Fig. 2F). Together, these results suggested that exogenous His-CYGB was internalized by the cells through the clathrin-mediated endocytosis pathway.

HIS-CYGB TRIGGERS THE DEACTIVATION OF HSCs AND SUPPRESSES COLLAGEN PRODUCTION *IN VITRO*

Next, we investigated the effects of exogenous His-CYGB on cultured HHSteCs. The addition of His-CYGB (5-80 μg/mL, for 1-48 hours) markedly suppressed the protein levels of HSC activation markers, including COL1A1 and αSMA (Fig. 3A). To examine changes in gene expression associated with the activation of HSCs and the function of His-CYGB, we performed RNA-seq analysis of three untreated and three His-CYGB–treated HHSteC samples. The RNA-seq data revealed that 215 genes were significantly changed by twofold or higher ($P < 0.05$) in the His-CYGB treatment group compared with the control group (Supporting Fig. S5A). Gene set enrichment analysis showed that gene ontology terms associated with biological processes, such as "response to stimulus" and "response to stress," were overrepresented among the differentially expressed genes (Supporting Fig. S5B). Consistently, RNA-seq data revealed the down-regulation of extracellular matrix–encoding and fibrosis-related genes, such as collagen type 21 alpha 1, collagen type 13 alpha 1, collagen type 14 alpha 1, and α*SMA*, and the up-regulation of antioxidant and matrix metalloproteinase (*MMP*) genes (*MMP-1*) in response to the

His-CYGB treatment (Fig. 3B). Quantitative RT-PCR (qRT-PCR) confirmed the significant down-regulation of fibrosis-related mRNA expression, such as of *αSMA* (50%), *COL1A1* (84%), *COL3A1* (66%), *TIMP-1* (64%), and *TGF-β1* (64%); however, *MMP-1* expression increased by 32-fold (Fig. 3C). Similar effects of the His-CYGB treatment were confirmed in cultured HHSteCs (Fig. 3D) and mHSCs (Fig. 3E, F). Interestingly, after the His-CYGB–containing medium was removed by washing the cells four times with PBS, His-CYGB could be detected in HHSteCs for at least 48 hours (Supporting Fig. S6A, B). COL1A1 levels, in both the culture medium and cell lysate, increased 12 hours after washing, and αSMA

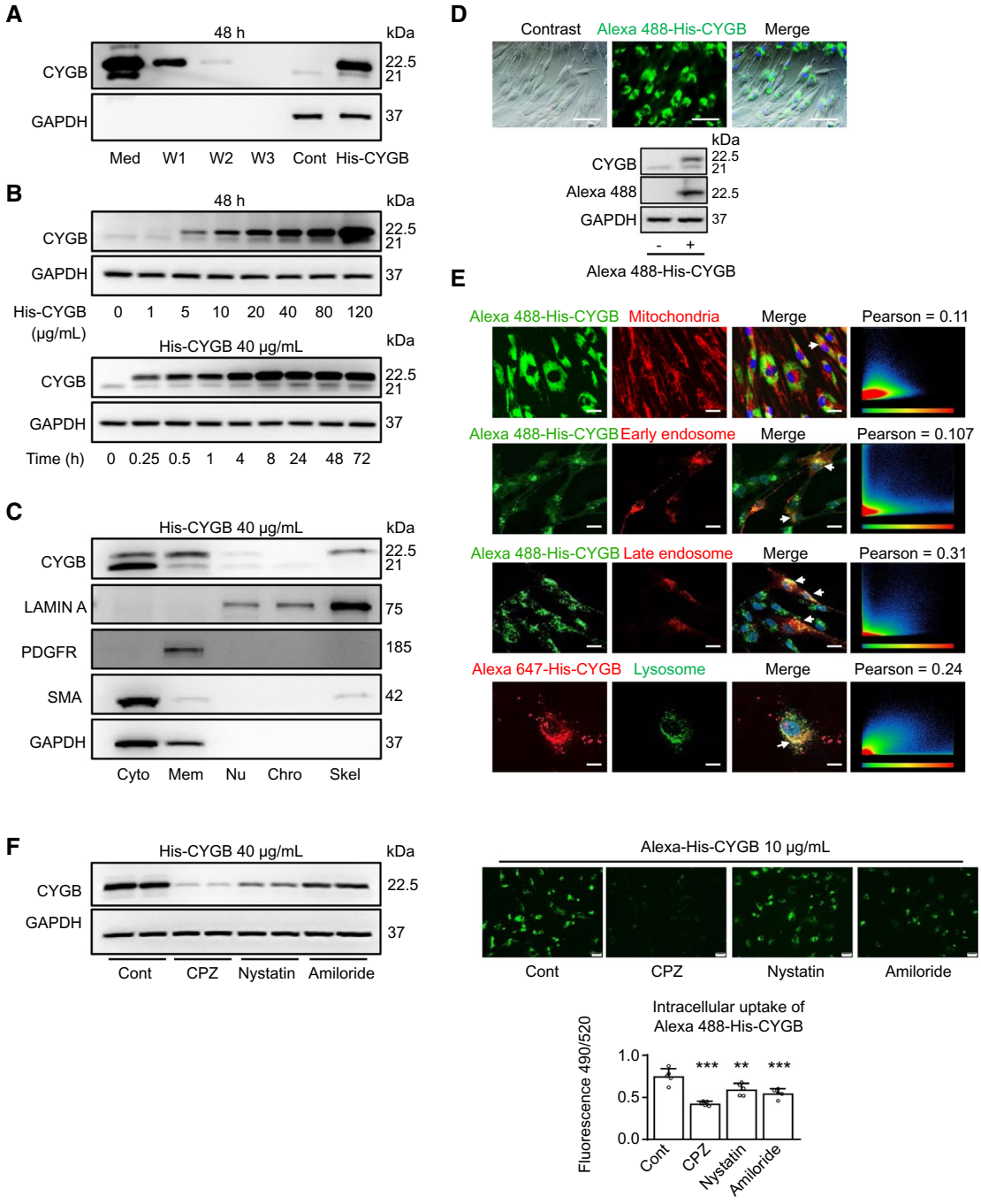

FIG. 2. His-CYGB production and its distribution *in vitro.* (A) Immunoblotting analysis for intracellular translocation of His-CYGB (40 μg/mL) into HHSteCs. The cells were treated with His-CYGB for 48 hours and then washed three times with PBS before collecting the cell lysate. All the medium, washing buffer, and cell lysate were collected for immunoblotting analysis. His-CYGB (22.5 kDa) presented above endogenous CYGB (21 kDa) in the cell lysate. (B) Dose- and time-dependent immunoblotting analysis for His-CYGB treatment in HHSteCs. (C) Immunoblotting analysis for fractionated cellular proteins. Cyto, Mem, Nu and Chro, and Skel markers were GAPDH, PDGFRβ, Lamin A, and αSMA, respectively. (D) Representative fluorescent images and immunoblotting analysis of the intracellular distribution of Alexa 488–His-CYGB (green, 10 μg/mL, 48 hours) in HHSteCs. Scale bars, 100 μm. (E) Confocal microscopic analysis of His-CYGB localization in HHSteCs. Representative fluorescent images of the double staining for Alexa 488–His-CYGB (green) or Alexa 647–His-CYGB (red) with organelle markers, including the mitochondria (red), early endosomes (red), late endosomes (red), and lysosomes (green). Scale bars, 20 μm. The Pearson correlation coefficient was shown. Hoechst 33258 (blue) was used to visualize nuclei. (F) Immunoblotting analysis (left panel) and representative fluorescent images (right panel) for the endocytosis inhibitor assay with their relative absorbance levels (bottom panel). His-CYGB or Alexa 488–His-CYGB and inhibitors of clathrin-mediated endocytosis (CPZ), caveolae-mediated endocytosis (nystatin), or macropinocytosis (amiloride) were treated simultaneously for 4 hours (n = 5). $^{**}P < 0.01$, and $^{***}P < 0.001$, one-way ANOVA followed by Tukey multiple comparison tests. Abbreviations: Med, medium in His-CYGB treated sample; W1-3, collected washing buffer (3 times) in His-CYGB treated sample; Cont, untreated; GAPDH, glyceraldehyde-3-phosphate dehydrogenase; Cyto, cytoplasmic. Abbreviations: Chro, chromatin bound; Cont, untreated control; Cyto, cytoplasmic; GAPDH, glyceraldehyde-3-phosphate dehydrogenase; Med, medium in His-CYGB–treated sample; Mem, plasma membrane; Nu, nuclear soluble; PDGFRβ, platelet derived growth factor receptor beta; Skel, cytoskeletal; W1-3, collected washing buffer (washed 3 times) in His-CYGB–treated sample.

reappeared in a time-dependent manner as being negatively correlated with His-CYGB decline. Because we found His-CYGB endocytosed through the clathrin-mediated pathway, we performed transient silencing of clathrin to clarify its involvement in the antifibrotic effect of His-CYGB. Interestingly, clathrin silencing at least partly blocked the His-CYGB effect by reverting *COL1A1* expression in HHSteCs (Supporting Fig. S6C).

HSC activation is triggered by TGF-β through mothers against decapentaplegic homolog 2/3 (SMAD2/3).[24] Here, we showed that recombinant (r)TGF-β1 induced the typical phosphorylation of SMAD3 for up to 48 hours after treatment in HHSteCs. The addition of His-CYGB (80 μg/mL) antagonized phosphorylated SMAD3 (pSMAD3) formation and attenuated both COL1A1 and αSMA expression at both protein and RNA levels (Supporting Fig. S7A, B). Thus, exogenous His-CYGB was demonstrated to interfere with the HSC activation process, even under conditions of recombinant TGF-β1 stimulation.

Next, we tested the effect of TAT-CYGB, as described in the Methods section. TAT-CYGB translocated into HHSteCs faster than His-CYGB (Supporting Fig. S8A, B). TAT-CYGB regulated fibrosis-related protein and mRNA expression levels in HHSteCs, which was similar to the effects observed with His-CYGB (Supporting Fig. S8C–E). These results confirmed that rhCYGB can penetrate into the cytoplasm and trigger the deactivation of HSCs *in vitro*, regardless of the selection or presence of a protein tag sequence.

HIS-CYGB SCAVENGES ROS AND ATTENUATES ROS-INDUCED HSC ACTIVATION AND COLLAGEN SYNTHESIS

CYGB is involved in the detoxification of ROS, nitric oxide metabolism, and lipid metabolism,[14,25,26] which are all associated with HSC activation and liver fibrogenesis. Herein, we directly demonstrated the ROS-scavenging function of His-CYGB. In a cell-free system, the total antioxidant capacity (TAC) of His-CYGB was equivalent to that of 1,094 nmol/μg of Trolox, a water-soluble vitamin E analogue (Fig. 4A, left). His-CYGB–treated HHSteCs demonstrated a significant TAC increase (by twofold) when compared with untreated controls (Fig. 4A, right). During the spontaneous, culture-dependent activation of HHSteCs, cellular ROS formation, which was measured using a 2′,7′-dichlorofluorescein diacetate (DCFDA)-based assay, increased in a time-dependent manner, demonstrating a fivefold increase on day 3 (Fig. 4B, left). The His-CYGB treatment suppressed ROS generation in a dose-dependent manner (Fig. 4B, right). H_2O_2 administration in HHSteCs induced a dose-dependent increase in hydroxyl radical ($OH^{\bullet}$) levels (Fig. 4C, top), which were scavenged by His-CYGB (Fig. 4C, bottom). Hypoxanthine (HX)–xanthine oxidase (XO) treatment increased superoxide anion radical ($O_2^{\bullet -}$) levels in a dose-dependent manner as measured by the superoxide selective fluorescent probe (BES-So assay) in a cell-free system (Fig. 4D, top). The addition of His-CYGB reduced more

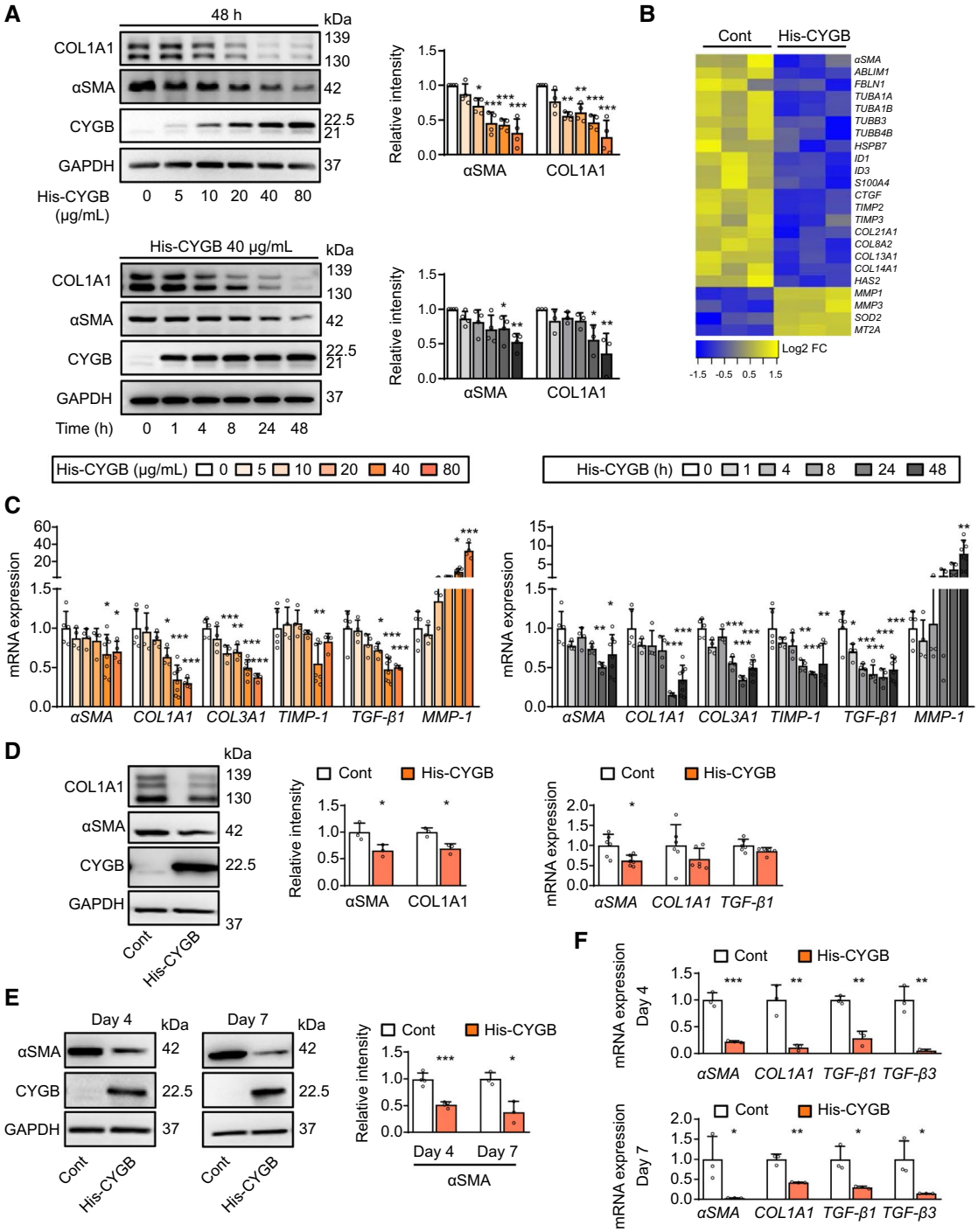

FIG. 3. His-CYGB triggers the deactivation and the suppression of collagen production in HHSteCs. (A) Dose-dependent (top panel) and time-dependent (bottom panel) immunoblotting analysis and quantifications of activated HHSteCs treated with His-CYGB. (B) Heatmap analysis of fibrosis- and antioxidant-related genes that were changed significantly (twofold) in HHSteCs treated with His-CYGB (80 μg/mL, 48 hours) compared with untreated controls by RNA-seq (n = 3). (C) Dose-dependent (left panel) and time-dependent (right panel) qRT-PCR analysis of activated HHSteCs treated with His-CYGB. (D) Immunoblotting analysis (left panel) and quantification (middle panel) and qRT-PCR analysis (right panel) of primary HHSteCs treated with His-CYGB (40 μg/mL, 48 hours). (E-F) Immunoblotting (E) and qRT-PCR (F) analysis of mHSCs (day 4 and day 7) treated with His-CYGB (40 μg/mL, 48 hours). $^{*}P < 0.05$, $^{**}P < 0.01$, and $^{***}P < 0.001$, one-way ANOVA followed by Tukey multiple comparison tests. Abbreviation: Cont, untreated control.

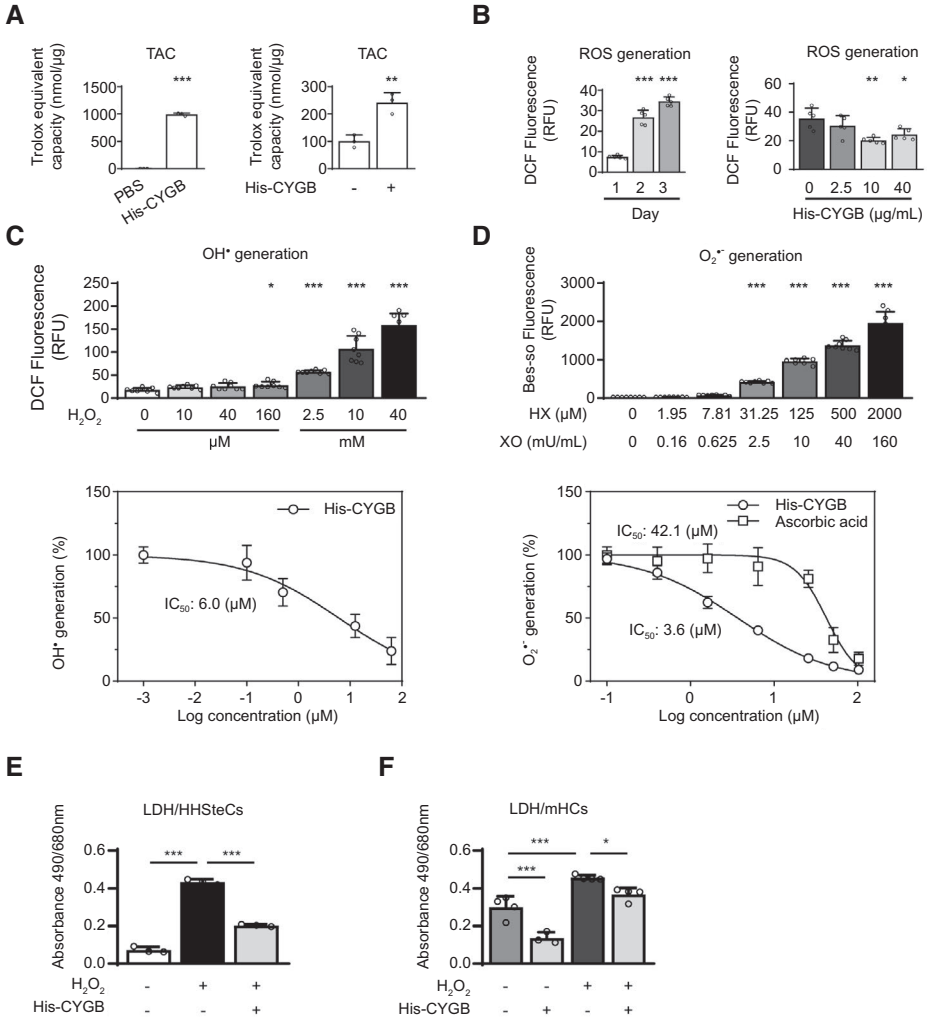

FIG. 4. His-CYGB scavenges ROS. (A) TAC assay in a cell-free system (left panel) and HHSteC cell lysates with or without His-CYGB treatment (40 μg/mL, 48 hours) (right panel). (B) Determination of intracellular ROS by DCFDA assay in activated HHSteCs under spontaneous condition (left panel) and His-CYGB treatment (48 hours, right panel). (C) Determination of $OH^{\bullet}$ generation by DCFDA assay in HHSteCs. The top panel shows $OH^{\bullet}$ generation under H_2O_2 dose-dependent stimulation (3 hours), and the bottom panel shows that His-CYGB dose-dependently blocks $OH^{\bullet}$ generated by 1 mM H_2O_2. (D) Determination of $O_2^{\bullet-}$ generation by BES-So assay in a cell-free system. The top panel shows HX-XO reaction–induced $O_2^{\bullet-}$ generation in a dose-dependent manner, and the bottom panel shows His-CYGB and ascorbic acid dose-dependently scavenger $O_2^{\bullet-}$ generated by HX (125 μM) and XO (10 mU/mL) challenge. (E-F) Measurement of ROS-induced LDH cytotoxicity in the HHSteCs (E) and mHCs (F) under His-CYGB treatment. His-CYGB (100 μg/mL) and H_2O_2 (1.5 mM) were treated simultaneously for 4 hours (HHSteCs) or for 2 hours (mHCs). $^{*}P < 0.05$, $^{**}P < 0.01$, and $^{***}P < 0.001$, Student *t* test or one-way ANOVA followed by Tukey multiple comparison tests. Abbreviations: IC50, the half-maximal inhibitory concentration; RFU, relative fluorescence unit.

than 90% of the $O_2^{\bullet-}$ released by the HX-XO reaction, which was a stronger effect than that observed for ascorbic acid at the same concentration (Fig. 4D, bottom). In addition, the His-CYGB treatment protected HHSteCs and mHCs from HX-XO- or H_2O_2-induced cellular toxicity (Fig. 4E, F).

Importantly, as shown in Fig. 5A, the stimulation of HHSteCs with either H_2O_2 or HX-XO increased the expression of αSMA and COL1A1 at the protein level. The His-CYGB treatment significantly blocked these effects (Fig. 5B). These results suggested that His-CYGB could scavenge endogenous

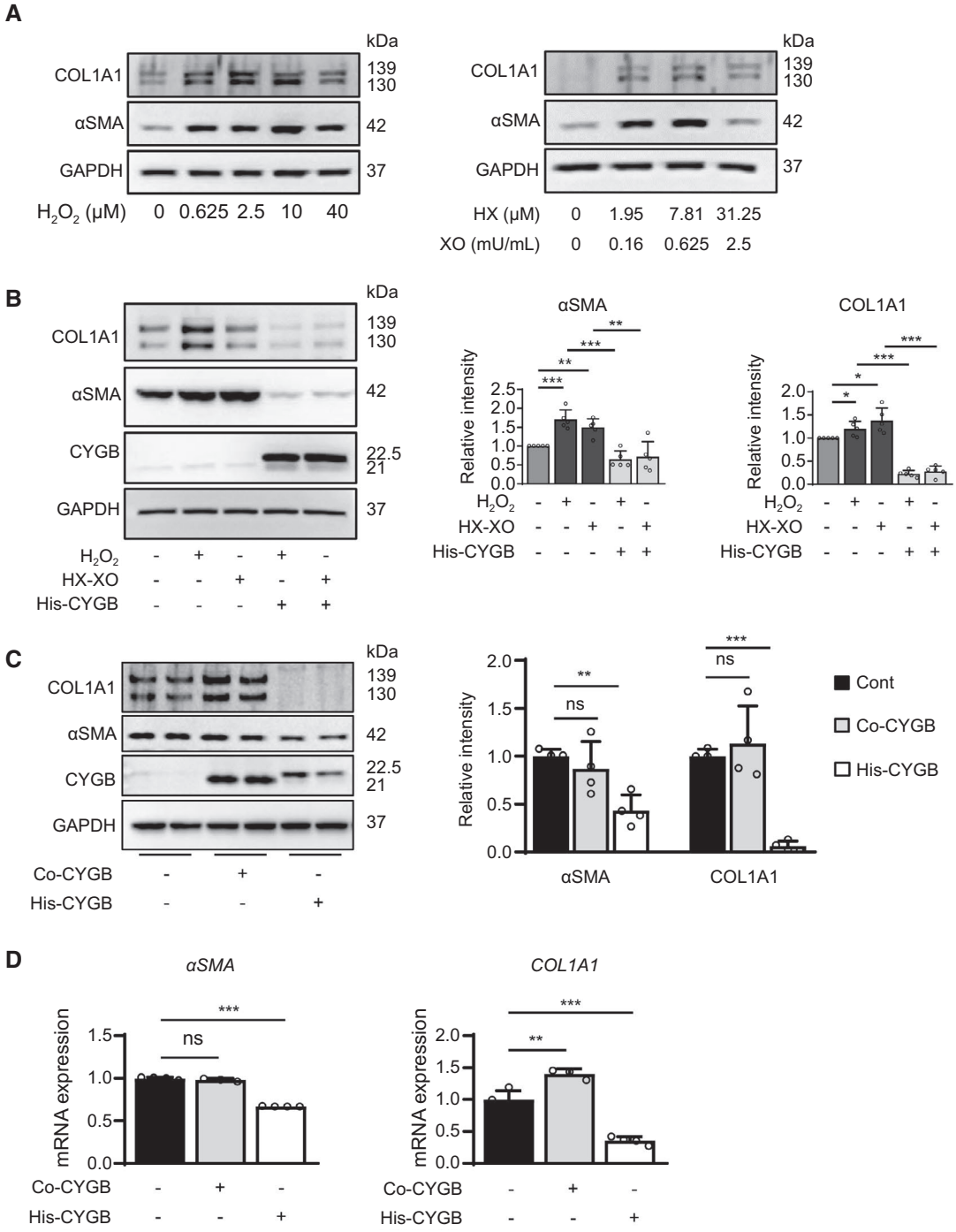

FIG. 5. His-CYGB attenuates ROS-induced HSC activation and collagen synthesis. (A) COL1A1 and αSMA expression in activated HHSteCs were increased under H_2O_2 (left panel) or HX-XO (right panel) administration for 48 hours. (B) Immunoblotting analysis of H_2O_2-induced (10 μM) or HX (7.81 μM) and XO (0.625 mU/mL)–induced activated HHSteCs without or with His-CYGB treatment (80 μg/mL, 48 hours) and their quantifications. (C-D) Replacement of the iron center of the heme group with cobalt ions (Co-CYGB) resulted in the loss of the His-CYGB effect. (C) Immunoblotting and (D) qRT-PCR analysis of HHSteCs treated with Co-CYGB in comparison with His-CYGB (40 μg/mL, 48 hours). $^{*}P < 0.05$, $^{**}P < 0.01$, and $^{***}P < 0.001$, one-way ANOVA followed by Tukey multiple comparison tests. Abbreviation: ns, not significant.

and exogenous ROS, resulting in the prevention of HSC activation.

To assess whether the ROS-scavenging function was specific for the heme-bound CYGB conformation, we replaced the iron center of the heme group with cobalt ions (Co-CYGB). Consequently, Co-CYGB failed to suppress the expression of COL1A1 and αSMA protein and mRNA, indicating that heme is crucial for CYGB function (Fig. 5C, D).

IFN-β IS INVOLVED IN THE HIS-CYGB–INDUCED DEACTIVATION OF HSCs

RNA-seq analysis of His-CYGB-treated HHSteC samples in comparison with controls revealed the down-regulation of the fibrosis-related genes as shown in Fig. 3B. Besides that, to our surprise, IFN-stimulated genes such as the genes encoding IFN-inducible (IFI) proteins *IFI27*, *IFI6*, and *IFI44L*; interferon-stimulated gene 15, the IFN regulatory factors (IRFs) *IRF7* and *IRF9*; and 2'-5'-oligoadenylate synthetase 2 (*OAS2*) were up-regulated, suggesting the involvement of IFN signaling during His-CYGB treatment (Fig. 6A, left). qRT-PCR analysis confirmed that these genes and their upstream targets, *STAT1/2*, *JAK1*, and nonreceptor tyrosine-protein kinase 2 (*TYK2*) were highly expressed, whereas the *COL1A1* and α*SMA* levels were suppressed (Fig. 6A, right).

The JAK/STAT pathway is known to be activated by IFNs.[27] We hypothesized that His-CYGB treatment affects IFN secretion in HSCs. As expected, His-CYGB (80 μg/mL) treatment increased the levels of phosphorylated (P-)TBK1, which is a key signaling molecule involved in IFN secretion,[28] during the early phase (0.5-1 hours) of the challenge (Fig. 6B). Subsequently, His-CYGB treatment in HHSteCs promoted the expression of *IFN-β*, but not *IFN-α* or *IFN-γ*, at the mRNA level (Fig. 6C, left). When IFN-β levels were measured in the culture media from HHSteCs, using an enzyme-linked immunosorbent assay (Fig. 6C, right), secreted IFN-β protein peaked at 4 hours and maintained high levels until 24 hours following the His-CYGB challenge. Simultaneous with IFN-β secretion, STAT1 phosphorylation was observed, 2-8 hours after His-CYGB challenge (Fig. 6B). Similarly, rhIFN-β (100 IU/mL) treatment leads to the induction of JAK/STAT pathway–associated mRNA sequences and the reduction of fibrosis-related gene expression in HHSteCs (Fig. 6D). In opposition, the JAK1-specific inhibitor momelotinib (N-(cyanomethyl)-4-{2-[4-(morpholin-4-yl) anilino]pyrimidin-4-yl}benzamide, CYT387), attenuated the phosphorylation of STAT1 and the reduction in COL1A1 production in both His-CYGB– and rhIFN-β–treated HHSteCs (Fig. 6E). These results suggested that His-CYGB promoted the secretion of IFN-β, which, in turn, activated JAK/STAT signaling in HHSteCs, synergically contributing to their deactivation (Fig. 6F).

SAFETY AND DISTRIBUTION OF HIS-CYGB *IN VIVO*

The safety of His-CYGB was assessed *in vivo* in both WT and PXB mice. The serum levels of mouse AST and ALT during the acute (1-48 hours) or chronic phases (2 weeks) in WT mouse (Fig. 7A) and human albumin (h-Alb) and ALT in PXB mice (Fig. 7B) did not change following the injection of His-CYGB, suggesting that His-CYGB administration resulted in negligible side effects for both mouse and human HCs.

The *in vivo* and *ex vivo* analysis of the injected Alexa 488–His-CYGB conjugates revealed the significant accumulation of the fluorescence signal in the liver, kidney, pancreas, fat, intestine, colon, stomach, and bladder, but not in the brain, for both normal WT mice and WT mice with TAA-induced liver fibrosis when assessed between 1 hour and 48 hours after injection (Fig. 7C, D). To our surprise, at the liver tissue level, Alexa 488–His-CYGB accumulated in hepatic sinusoidal cells (Fig. 7E), colocalized with desmin-positive HSCs, and partially colocalized with cluster of differentiation 31 (CD31)–positive endothelial cells but did not colocalize with CD68-positive macrophages (Fig. 7F-top). To verify these findings, *Cygb*-deficient mice were injected with His-CYGB, and its distribution was determined using an anti-CYGB antibody. Consistently, His-CYGB was found in HSCs and endothelial cells, but not macrophages, in both untreated and CDAA-treated *Cygb*-deficient mice (Fig. 7F, bottom; Supporting Fig. S9A). In the kidney, His-CYGB localized in the glomerulus and along the tubules (Supporting Fig. S9B). Then, we used 5-nm Ni-NTA nanogold particles to label His-CYGB proteins using a postembedding labeling method and observed the localization of His-CYGB by TEM. Consistent with Alexa labeling, nanogold

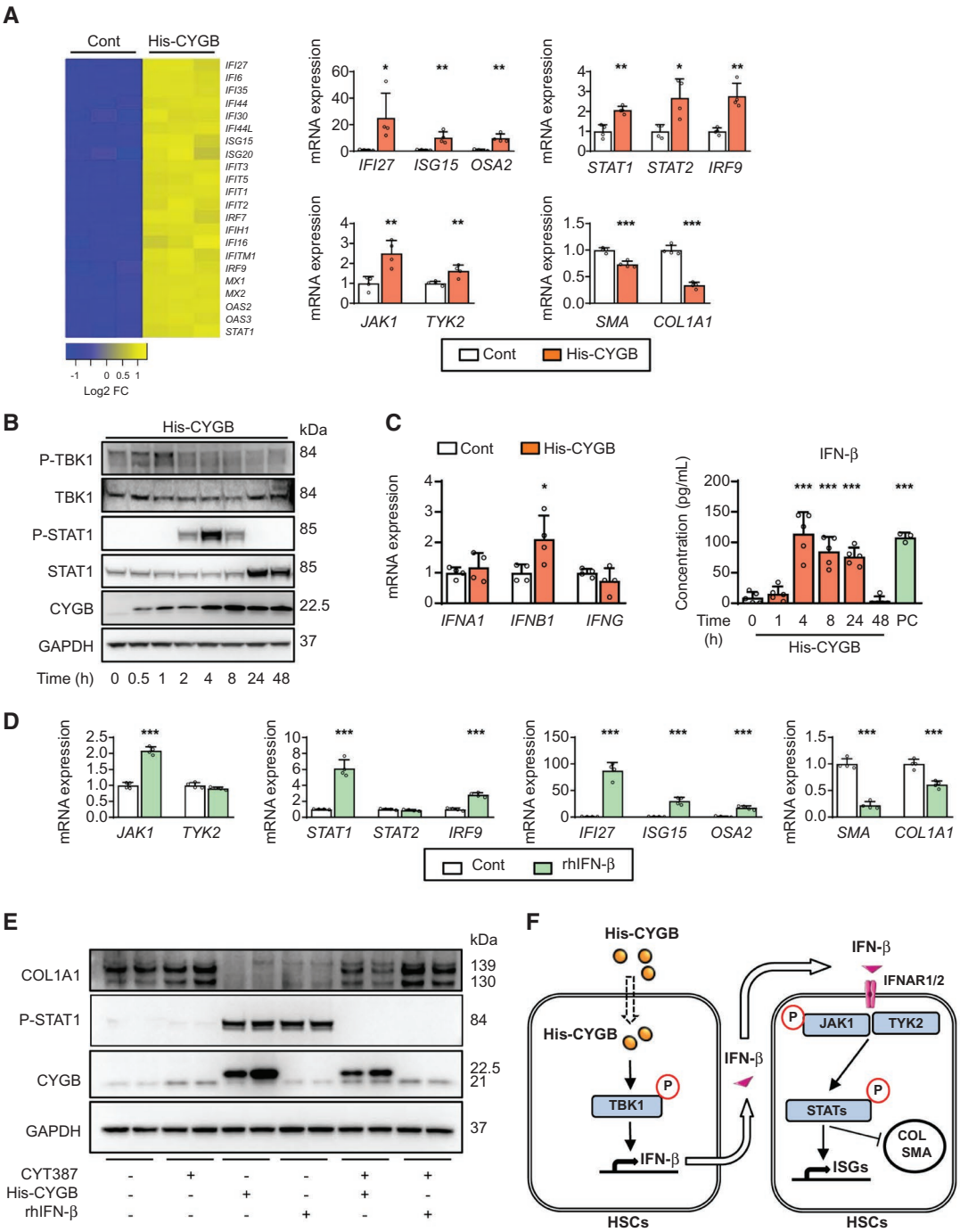

FIG. 6. His-CYGB selectively induces IFN-β. (A) Heatmap analysis by RNA-seq (left panel) and qRT-PCR analysis (right panel) of IFN pathway–related genes (n = 3) in HHSteCs treated with His-CYGB (80 μg/mL, 48 hours) compared with untreated controls. (B) Time-dependent immunoblotting analysis of HHSteCs with His-CYGB treatment (80 μg/mL). (C) qRT-PCR of HHSteCs with His-CYGB treatment (80 μg/mL, 48 hours) (left panel). Level of IFN-β in cultured media of His-CYGB–treated HHSteCs (40 μg/mL) by ELISA (n = 5) (right panel). rhIFN-β (100 IU/mL) serves as a PC. (D) qRT-PCR analysis of HHSteCs under rhIFN-β treatment (100 IU/mL, 48 hours). (E) Immunoblotting analysis of HHSteCs that were preincubated with or without the JAK1 inhibitor momelotinib (CYT387, 2 μM, 24 hours) following with or without His-CYGB (80 μg/mL) or rhIFN-β (100 IU/mL) for 48 hours. (F) A proposed scheme illustrating the effect of His-CYGB on the IFN-β pathway in HSCs. *$P < 0.05$, **$P < 0.01$, ***$P < 0.001$, two-tailed Student t test or one-way ANOVA. Abbreviations: Cont, untreated control; COL, collagen; FC, fold change; IFNAR, interferon-α/β receptor; P, phosphorylated; PC, positive control.

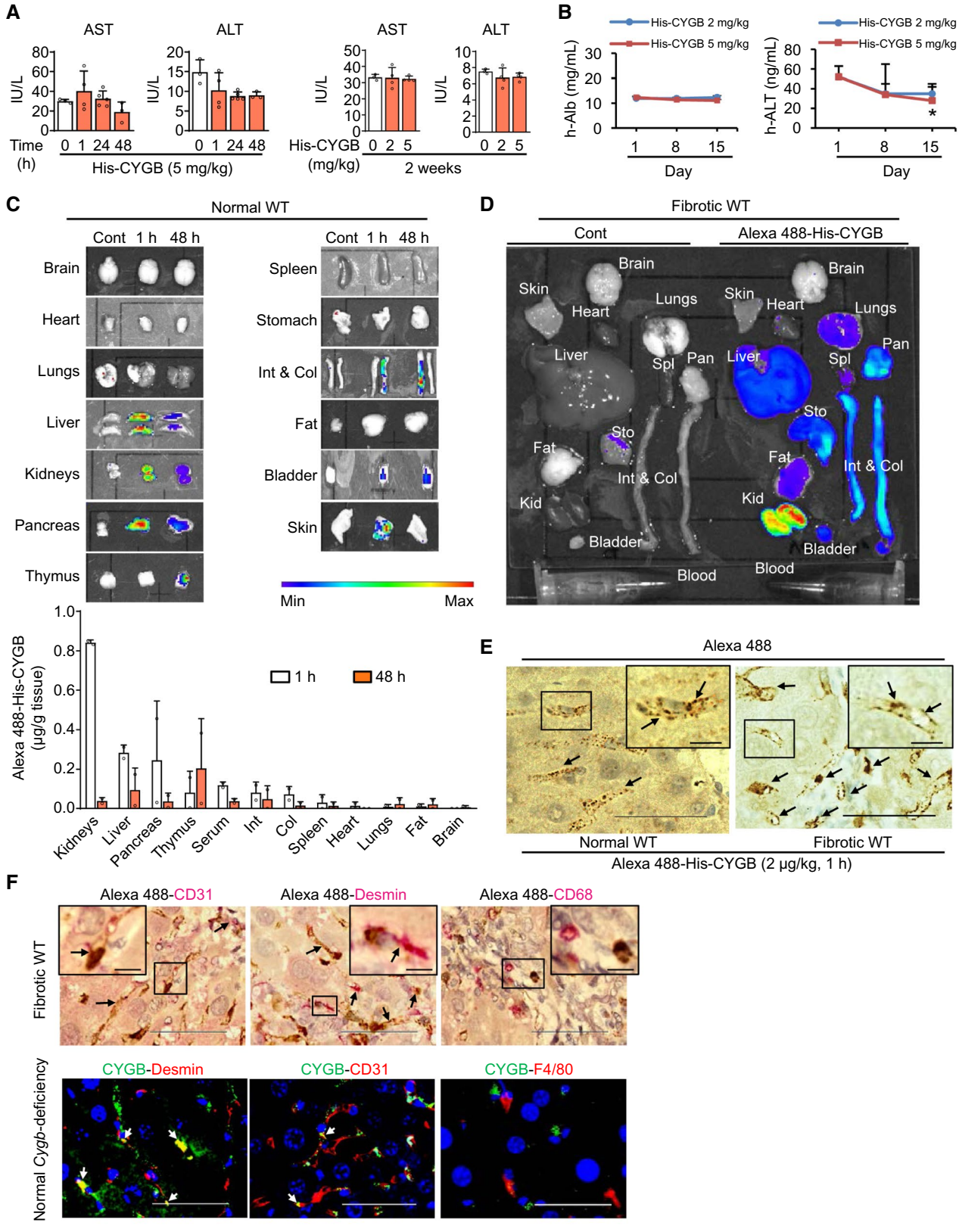
A
AST
ALT
AST
ALT
IU/L
Time (h)
0 1 24 48
His-CYGB (5 mg/kg)
His-CYGB (mg/kg)
0 2 5
2 weeks
B
His-CYGB 2 mg/kg
His-CYGB 5 mg/kg
h-Alb (mg/mL)
h-ALT (ng/mL)
Day
C
Normal WT
Cont 1 h 48 h
Brain
Heart
Lungs
Liver
Kidneys
Pancreas
Thymus
Spleen
Stomach
Int & Col
Fat
Bladder
Skin
Min
Max
Alexa 488-His-CYGB (μg/g tissue)
1 h
48 h
Kidneys
Liver
Pancreas
Thymus
Serum
Int
Col
Spleen
Heart
Lungs
Fat
Brain
D
Fibrotic WT
Cont
Alexa 488-His-CYGB
Sto
Kid
Blood
E
Alexa 488
Normal WT
Fibrotic WT
Alexa 488-His-CYGB (2 μg/kg, 1 h)
F
Alexa 488-CD31
Alexa 488-Desmin
Alexa 488-CD68
Fibrotic WT
CYGB-Desmin
CYGB-CD31
CYGB-F4/80
Normal Cygb-deficiency

FIG. 7. Safety and distribution of His-CYGB *in vivo*. (A) Serum levels of mouse AST and ALT of normal WT mice under His-CYGB treatment for 1-48 hours (left panel) and 2 weeks (right panel) (n = 3-5). (B) Serum levels of h-Alb and h-ALT of PXB mice under His-CYGB treatment for 2 weeks (n = 3). (C) Representative fluorescent images of the Alexa 488–His-CYGB in normal WT mice at 1 hour or 48 hours after injection (top panel) and distribution of fluorescence signal in different organs (bottom panel) (n = 2). (D) Representative fluorescent images of the Alexa 488–His-CYGB in fibrotic WT mice at 1 hour after injection. (E) IHC staining for Alexa 488–positive cells (black arrows) in the liver. Scale bars, 50 μm; inset, 10 μm. (F) Assessment for cellular colocalization of Alexa 488–His-CYGB in the liver of fibrotic WT mice (top panel) and His-CYGB in the liver of normal *Cygb*-deficient mice (bottom panel). In double IHC staining (top panel), black arrows indicate double-positive cells for Alexa (brown) and CD31 (pink). In double immunofluorescence staining (bottom panel), white arrows indicate double-positive cells for His-CYGB (green) and desmin (red), CD31 (red), or F4/80 (red). DAPI (blue) was used to visualize nuclei. Scale bars, 50 μm; inset, 10 μm. **P* < 0.05, day 15 versus day 1 of 5-mg/kg His-CYGB treatment groups in B, Student *t* test. F4/80 as a macrophage marker.

particle–labeled His-CYGB was found predominantly on the outer membrane of the mitochondria in HSCs and was partially localized on endothelial cells and HCs (Supporting Fig. S9C-E).

HIS-CYGB PROTECTS MICE FROM LIVER INJURY AND FIBROSIS

Next, the applicability of His-CYGB as protein therapy against liver injury and fibrosis was tested using *in vivo* mouse models. The appropriate dose of His-CYGB was first determined by evaluating liver cirrhosis in mice that had already developed severe liver fibrosis because of the injection of TAA (Supporting Fig. S10A). The blood biochemistry analysis (Supporting Fig. S10B) showed that remaining organ functions, including kidney function, ascertain the safety of the His-CYGB treatment. Serum levels of AST, ALT, and lactate dehydrogenase (LDH) were all significantly diminished following the His-CYGB treatment (Fig. 8A). Histological analysis revealed that the His-CYGB treatment inhibited the infiltration of neutrophils and CD68-positive macrophages in the liver when compared with controls (Fig. 8B). RNA-seq analysis revealed that 125 genes were significantly up-regulated or down-regulated by twofold or higher ($P < 0.05$) in the His-CYGB treatment group compared with the control group (Supporting Fig. S10C). In results similar to the RNA-seq results *in vitro*, we found that gene ontology terms associated with biological processes, such as "response to stimulus" and "response to stress," were overrepresented among the differentially expressed genes (Supporting Fig. S10D). The expression of cytochrome P450 (Cyp) family genes, such as *Cyp1a1*, *Cyp1a2*, *Cyp2b10*, *Cyp3a11*, *Cyp3a13*, and *Cyp3a16*, remained unchanged in His-CYGB–treated mice (Supporting Table S4), indicating the safety of the His-CYGB treatment. Interestingly, all of the typical fibrosis-related genes and genes associated with inflammatory cytokines, inflammatory chemokines, and the oxidative stress response were significantly down-regulated (Fig. 8C), which was confirmed by qRT-PCR analysis (Fig. 8D). Consistently, His-CYGB inhibited the TAA-induced deposition of collagen (Sirius red and fast green [SiR-FG] staining and quantification; Fig. 8B and Supporting Fig. S11A). Furthermore, it significantly suppressed up to 72% of COL1A1 and 78% of αSMA at protein and RNA levels and 43% of *Tgf-β1*, 53% of *Tgf-β3*, and 79% of *Timp-1* mRNA expression (Supporting Fig. S11B and Fig. 8D). Reduced glutathione (GSH) is among the most important ROS scavengers, and the ratio of GSH to oxidized glutathione (GSSG) is widely used in clinical practice to evaluate the oxidative stress status of biological samples.[29] Reduced GSSG concentrations and increased GSH/GSSG ratios in the liver tissue of His-CYGB–treated mice indicated high antioxidant capacity (Fig. 8E). The levels of lipid peroxidation, 4-HNE, and DNA damage markers, including phosphorylated H2A histone family member X (γ-H2AX) and 8-hydroxy-2'-deoxyguanosine (8-OHdG), were significantly reduced following the His-CYGB treatment (Fig. 8B, F).

To further support and extend the application of our data, we examined whether the His-CYGB treatment could protect the liver from DDC-induced cholestasis (Supporting Fig. S12A). His-CYGB exerted protective effects in this liver disease model that were similar to those observed in other models, including reduced injury (Supporting Fig. S12B) and anti-inflammatory, antifibrotic (Supporting Fig. S12C,

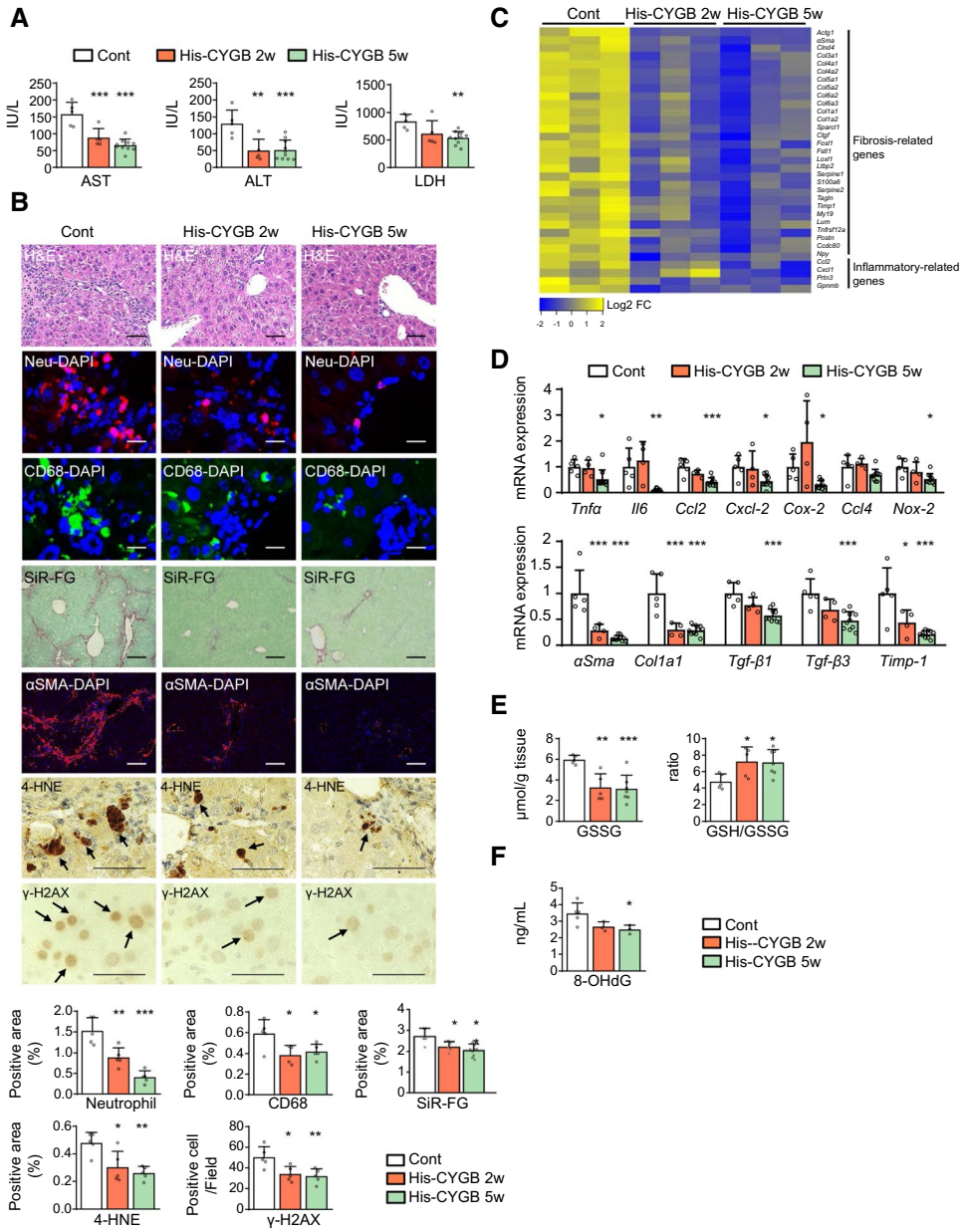

FIG. 8. His-CYGB administration prevents the aggravation of TAA-induced liver inflammation and fibrosis. The experiment design is shown in Supporting Fig. S10A. (A) Serum levels of AST, ALT, and LDH (n = 5-10). (B) Representative liver images of H&E, immunofluorescence, SiR-FG, and IHC staining and their quantifications (n = 4-5). Neu are shown in red, CD68 is shown in green, and αSMA is shown in red. DAPI (blue) was used to visualize nuclei. Scale bars, 50 μm. (C) Heatmap analysis of fibrosis- and inflammation-related genes that were changed significantly (twofold) by RNA-seq (n = 3). (D) qRT-PCR analysis for inflammation-related genes (top) and fibrosis-related genes (bottom) in the liver (n = 4-10). (E) Glutathione assay for GSSG and GSH/GSSG in the liver (n = 5-7). (F) Liver 8-OHdG content by ELISA (n = 3-5). *P < 0.05, **P < 0.01, and ***P < 0.001, one-way ANOVA followed by Tukey multiple comparison tests. Abbreviation: Cont, untreated control.

D), and antioxidant effects (Supporting Fig. S12E). When RNA-seq analysis was performed on livers of His-CYGB–treated, DDC-fed mice, inflammatory and fibrosis-related genes were down-regulated, whereas antioxidant and retinoid metabolism genes associated with quiescent HSCs were up-regulated,

compared with only DDC-fed mice (Supporting Fig. S12F). These findings indicated that the His-CYGB treatments could attenuate liver injury, inflammation, and cirrhosis development.

Finally, STAT1 phosphorylation was examined 1 hour after His-CYGB or normal saline injection in TAA-treated (10 weeks) fibrotic WT mice. As expected, P-STAT1–positive cells were found among the nonparenchymal cells in fibrotic septa in His-CYGB–treated mice but were absent in saline-treated controls (Supporting Fig. S13), implying the possible activation of IFN-β/JAK/STAT pathway *in vivo* under His-CYGB therapy.

Discussion

More than 130 different proteins or peptides have been approved for clinical use by the U.S. Food and Drug Administration to treat or alleviate diseases, including insulin, growth hormone, factor VIII, h-Alb, and (rh) interferons.[30] However, many antifibrotic therapeutic agents cannot be clinically applied because they do not target HSCs and are toxic to parenchymal cells.[31] Furthermore, many proteins are larger than the typical pore sizes between endothelial cells, and the distribution of proteins is therefore limited to the vascular space in the absence of specific protein receptors.[30] However, interestingly, peroxidases such as catalase, *Mpo*, and heme proteins with peroxidase activity, including hemoglobin, myoglobin and cytochrome c, have been extensively used in studies to trace the capillary permeability of various tissues.[32,33] Herein, we reported that exogenous His-CYGB protein is taken up by the clathrin-mediated endocytosis pathway and translocated into HSCs, both *in vitro* and *in vivo* (Fig. 2 and 7 and Supporting Fig. S4 and S9). The specific endocytosis of CYGB protein by HSCs but not Kupffer cells is of particular interest. Following injection, some His-CYGB molecules are absorbed by endothelial cells or HCs, but the majority make their way "home" to HSCs.

CYGB plays several roles, such as the detoxification of ROS and protection from apoptosis, and may be involved in lipid metabolism.[14,25,26] Recently, in a study involving human patients with nonalcoholic steatohepatitis, Okina et al. reported that $OH^{\bullet}$-dependent oxidative DNA damage in activated HSCs was caused by the TGF-β–dependent reduction of CYGB.[34] Our results directly showed that His-CYGB can scavenge many types of ROS (H_2O_2, $OH^{\bullet}$, and $O_2^{\bullet -}$) in both cell-based and cell-free systems, resulting in the significant inhibition of ROS-induced HSC activation and HC apoptosis (Fig. 4 and 5). The protective evidence of CYGB, as demonstrated in models of NASH disease, cholestatic cirrhosis, chemical cirrhosis, and biliary metabolic disorder, suggests that both the administration of His-CYGB protein and the overexpression of *Cygb* can defend both HSCs and HCs against liver damage induced by different etiologies.

Fibrogenic progression is associated with a significant decrease and/or depletion of antioxidant defense, and antioxidant supplementation can prevent fibrogenic progression. The drug that has been used to treat acetaminophen overdose in patients is the GSH precursor *N*-acetyl cysteine.[35] Vitamin E is reportedly effective for both alcohol-associated steatohepatitis– and NASH-induced fibrosis, thus improving histological findings, such as steatosis, inflammation, and fibrosis.[36] Our data indicated that the His-CYGB protein has a stronger antioxidant capacity than vitamin C for scavenging $O_2^{\bullet -}$ (Fig. 4D). Together, the demonstrated safety of His-CYGB (Fig. 7); its effects on the recovery of antioxidant enzymes and/or compounds in the liver, as shown by the increased GSH/GSSG ratio (Fig. 8E) and increased *Atx-1* and *Nat-8* expression (Fig. 1F); and the reduced production of $OH^{\bullet}$ and $O_2^{\bullet -}$ (Fig. 4) suggested that the His-CYGB protein represents a promising antioxidant approach for treating liver fibrosis and cirrhosis in humans.

Discovered in 1957, IFNs are now known to display antiviral activities, with a spectrum of clinical effectivities against both RNA- and DNA-based viruses, in addition to acting as prototypic biological response modifiers during cancer, sclerosis, and fibrosis.[37] Type 1 IFNs, such as IFN-α and IFN-β, are well-known drugs used for the treatment of chronic HCV infections[38] and preventing hepatic injury,[20] fibrosis,[39] and carcinogenesis.[40] This study demonstrated a link between His-CYGB and the IFN-β pathway. Besides its main function as a ROS scavenger, the His-CYGB protein additionally triggers HSC deactivation by activating the TBK1/IFN-β/JAK/STAT axis. Although we have not yet unraveled how His-CYGB induces the phosphorylation of TBK1 in HSCs, ROS production may interfere with TBK1-induced IFN-β secretion by oxidizing the stimulator of IFN genes (STING).[41] The scavenging of ROS

by CYGB may protect STING from oxidation, promoting IFN-β secretion. However, these features should be clarified in future studies.

Previously, rhCYGB was shown to reverse CCl_4-induced liver fibrosis in rats[42]; however, the safety, underlying mechanisms, specific targets, and effects of rhCYGB on HSCs have remained unexplored. Herein, we showed that His-CYGB administration is safe and has no significant adverse effects following administration in both WT and PXB mice. The PXB mouse model is a chimeric mouse, wherein more than 70% of the liver has been replaced with normal human HCs, and it is thus often used to conduct studies for drug development.[43] In our model of PXB mice, the His-CYGB treatment was not only safe for HC function (based on albumin levels) but also significantly improved ALT levels compared with control animals (Fig. 7B). In the TAA model, His-CYGB–injected mice showed no effects on the function of other organs, and it even lowered the level of blood urea nitrogen compared with control (Supporting Fig. S10B). Moreover, an Alexa 488–His-CYGB signal was not found in the brain, which suggested that His-CYGB could not pass through the blood–brain barrier. These results suggest a positive safety profile for His-CYGB.

In addition to tissue and cellular specificity, the dosing and timing of treatments are also important. We demonstrated that the reductions in COL1A1 production and HSC activation lasted for at least 48 hours *in vitro* (Supporting Fig. S6A, B) following the His-CYGB treatment; thus, injections of His-CYGB administered twice per week were used to determine the efficiency *in vivo*. The dose in our study (2 mg/kg of body weight) was lower than doses shown to have *in vivo* therapeutic effects.[42] Another important finding of our data was the up-regulation of *MMP1* expression in HHSteCs following the His-CYGB treatment (Fig. 3B, C). Although the mechanism underlying this function remains unclear, these data reflected the deactivated status of HSCs following the His-CYGB treatment, which promotes MMP activity and may be associated with the fibrosis regression observed in TAA and DDC models. Finally, CYGB exerted clear protective functions in various mouse models of liver injury, including BDL, steatohepatitis, TAA-induced fibrosis, and DDC-induced cholestasis. The consistency of these findings across multiple models indicated the applicability of His-CYGB for liver protection, regardless of the etiology of liver fibrosis.

Although our findings indicated that His-CYGB was mainly taken up by HSCs, whether HSCs express receptors that bind to His-CYGB remains to be determined. Notably, when examining other members of the globin family, Gburek et al. reported the plausible role of HC ectopic F-type domain 1-ATPase as a receptor for the endocytosis of hemoglobin.[44] Thus, future expanded studies examining CYGB-specific receptors may provide a more in-depth exploration of the HSC deactivation process.

In conclusion, our study provided insights into the mechanistic actions through which CYGB inhibits HSC activation status and liver fibrosis. The administration of His-CYGB could prevent liver injury and fibrosis in multiple experimental models of advanced chronic liver diseases. His-CYGB may potentially be developed for the treatment of human liver fibrosis.

Acknowledgment: We thank Dr. Kazuo Ikeda, Dr. Tsutomu Matsubara, and Mr. Yoshinori Okina for their helpful discussion and thank Dr. Hideto Yuasa for his technical help. Quantitative RT-PCR analysis was performed at the Research Support Platform of the Graduate School of Medicine at Osaka City University.

REFERENCES

1) Friedman SL. Mechanisms of hepatic fibrogenesis. Gastroenterology 2008;134:1655-1669.
2) Lee Y, Friedman SL. Fibrosis in the liver: acute protection and chronic disease. Prog Mol Biol Transl Sci 2010;97:151-200.
3) Comporti M, Saccocci C, Dianzani MU. Effect of CCl-4 in vitro and in vivo on lipid peroxidation of rat liver homogenates and subcellular fractions. Enzymologia 1965;29:185-204.
4) Ghoshal AK, Recknagel RO. Positive evidence of acceleration of lipoperoxidation in rat liver by carbon tetrachloride: In vitro experiments. Life Sci 1965;4:1521-1530.
5) Kamimura S, Gaal K, Britton RS, Bacon BR, Triadafilopoulos G, Tsukamoto H. Increased 4-hydroxynonenal levels in experimental alcoholic liver disease: association of lipid peroxidation with liver fibrogenesis. Hepatology 1992;16:448-453.
6) Friedman SL, Neuschwander-Tetri BA, Rinella M, Sanyal AJ. Mechanisms of NAFLD development and therapeutic strategies. Nat Med 2018;24:908-922.
7) Gualdi R, Casalgrandi G, Montosi G, Ventura E, Pietrangelo A. Excess iron into hepatocytes is required for activation of collagen type I gene during experimental siderosis. Gastroenterology 1994;107:1118-1124.
8) Farinati F, Cardin R, D'Errico A, De Maria N, Naccarato R, Cecchetto A, et al. Hepatocyte proliferative activity in chronic liver damage as assessed by the monoclonal antibody MIB1 Ki67 in archival material: the role of etiology, disease activity, iron, and lipid peroxidation. Hepatology 1996;23:1468-1475.

9) **Montfort CV**, **Matias N**, Fernandez A, Fucho R, de la Rosa LC, Martinez-Chantar ML, et al. Mitochondrial GSH determines the toxic or therapeutic potential of superoxide scavenging in steatohepatitis. J Hepatol 2012;57:852-859.
10) MacMillan-Crow L, Cruthirds D. Invited review: Manganese superoxide dismutase in disease. Free Radic Res 2001;34:325-336.
11) Urtasun R, Nieto N. Hepatic stellate cells and oxidative stress. Rev Esp Enferm Dig 2007;99:223-230.
12) Hernandez-Gea V, Friedman SL. Pathogenesis of liver fibrosis. Annu Rev Pathol 2011;6:425-456.
13) Kawada N, Kristensen DB, Asahina K, Nakatani K, Minamiyama Y, Seki S, et al. Characterization of a stellate cell activation-associated protein (STAP) with peroxidase activity found in rat hepatic stellate cells. J Biol Chem 2001;276:25318-25323.
14) Le Thuy TT, Hai NT, Hai H, Kawada N. Pathophysiological role of cytoglobin, the fourth globin in mammals, in liver diseases. Histol Histopathol 2016;31:257-267.
15) De Backer J, Razzokov J, Hammerschmid D, Mensch C, Hafideddine Z, Kumar N, et al. The effect of reactive oxygen and nitrogen species on the structure of cytoglobin: a potential tumor suppressor. Redox Biol 2018;19:1-10.
16) Thuy LTT, Matsumoto Y, Thuy TTV, Hai H, Suoh M, Urahara Y, et al. Cytoglobin deficiency promotes liver cancer development from hepatosteatosis through activation of the oxidative stress pathway. Am J Pathol 2015;185:1045-1060.
17) Thuy LTT, Van Thuy TT, Matsumoto Y, Hai H, Ikura Y, Yoshizato K, et al. Absence of cytoglobin promotes multiple organ abnormalities in aged mice. Sci Rep 2016;6:24990.
18) **Thi Thanh Hai N**, **Thuy LTT**, Shiota A, Kadono C, Daikoku A, Hoang DV, et al. Selective overexpression of cytoglobin in stellate cells attenuates thioacetamide-induced liver fibrosis in mice. Sci Rep 2018;8:17860.
19) Gao B, Wang H, Lafdil F, Feng D. STAT proteins - key regulators of anti-viral responses, inflammation, and tumorigenesis in the liver. J Hepatol 2012;57:430-441.
20) Tanabe J, Izawa A, Takemi N, Miyauchi Y, Torii Y, Tsuchiyama H, et al. Interferon-beta reduces the mouse liver fibrosis induced by repeated administration of concanavalin A via the direct and indirect effects. Immunology 2007;122:562-570.
21) **Van Thuy TT**, **Thuy LTT**, Yoshizato K, Kawada N. Possible Involvement of nitric oxide in enhanced liver injury and fibrogenesis during cholestasis in cytoglobin-deficient mice. Sci Rep 2017;7:41888.
22) Motoyama H, Komiya T, Thuy LTT, Tamori A, Enomoto M, Morikawa H, et al. Cytoglobin is expressed in hepatic stellate cells, but not in myofibroblasts, in normal and fibrotic human liver. Lab Invest 2014;94:192-207.
23) Thi Thanh Thuy LE, Morita T, Yoshida K, Wakasa K, Iizuka M, Ogawa T, et al. Promotion of liver and lung tumorigenesis in DEN-treated cytoglobin-deficient mice. Am J Pathol 2011;179:1050-1060.
24) Dooley S, ten Dijke P. TGF-β in progression of liver disease. Cell Tissue Res 2012;347:245-256.
25) Hankeln T, Ebner B, Fuchs C, Gerlach F, Haberkamp M, Laufs T, et al. Neuroglobin and cytoglobin in search of their role in the vertebrate globin family. J Inorg Biochem 2005;99:110-119.
26) Liu X, El-Mahdy MA, Boslett J, Varadharaj S, Hemann C, Abdelghany TM, et al. Cytoglobin regulates blood pressure and vascular tone through nitric oxide metabolism in the vascular wall. Nat Commun 2017;8:14807.
27) Ivashkiv LB, Donlin LT. Regulation of type I interferon responses. Nat Rev Immunol 2014;14:36-49.
28) Mogensen TH. IRF and STAT Transcription factors - from basic biology to roles in infection, protective immunity, and primary immunodeficiencies. Front Immunol 2019;9.
29) Zitka O, Skalickova S, Gumulec J, Masarik M, Adam V, Hubalek J, et al. Redox status expressed as GSH:GSSG ratio as a marker for oxidative stress in paediatric tumour patients. Oncol Lett 2012;4:1247-1253.
30) Leader B, Baca QJ, Golan DE. Protein therapeutics: a summary and pharmacological classification. Nat Rev Drug Discov 2008;7:21-39.
31) Bataller R, Brenner DA. Liver fibrosis. J Clin Invest 2005;115:209-218.
32) Anderson WA. The use of exogenous myoglobin as an ultrastructural tracer. Reabsorption and translocation of protein by the renal tubule. J Histochem Cytochem 1972;20:672-684.
33) Graham RC, Karnovsky MJ. Glomerular permeability. Ultrastructural cytochemical studies using peroxidases as protein tracers. J Exp Med 1966;124:1123-1134.
34) **Okina Y**, **Sato-Matsubara M**, Matsubara T, Daikoku A, Longato L, Rombouts K, et al. TGF-beta1-driven reduction of cytoglobin leads to oxidative DNA damage in stellate cells during non-alcoholic steatohepatitis. J Hepatol 2020;73:882-895.
35) Knight TR, Ho Y-S, Farhood A, Jaeschke H. Peroxynitrite is a critical mediator of acetaminophen hepatotoxicity in murine livers: protection by glutathione. J Pharmacol Exp Ther 2002;303:468-475.
36) Hasegawa T, Yoneda M, Nakamura K, Makino I, Terano A. Plasma transforming growth factor-beta1 level and efficacy of alpha-tocopherol in patients with non-alcoholic steatohepatitis: a pilot study. Aliment Pharmacol Ther 2001;15:1667-1672.
37) Borden EC, Sen GC, Uze G, Silverman RH, Ransohoff RM, Foster GR, et al. Interferons at age 50: past, current and future impact on biomedicine. Nat Rev Drug Discov 2007;6:975-990.
38) Ikeda F, Shimomura H, Miyake M, Fujioka SI, Itoh M, Takahashi A, et al. Early clearance of circulating hepatitis C virus enhanced by induction therapy with twice-a-day intravenous injection of IFN-beta. J Interferon Cytokine Res 2000;20:831-836.
39) Roh YS, Park S, Kim JW, Lim CW, Seki E, Kim B. Toll-like receptor 7-mediated type I interferon signaling prevents cholestasis- and hepatotoxin-induced liver fibrosis. Hepatology 2014;60:237-249.
40) Soga K, Shibasaki K, Aoyagi Y. Effect of interferon on incidence of hepatocellular carcinoma in patients with chronic hepatitis C. Hepatogastroenterology 2005;52:1154-1158.
41) Jin L, Lenz LL, Cambier JC. Cellular reactive oxygen species inhibit MPYS induction of IFNbeta. PLoS One 2010;5:e15142.
42) Li Z, Wei W, Chen B, Cai G, Li X, Wang P, et al. The effect of rhCygb on CCl4-induced hepatic fibrogenesis in rat. Sci Rep 2016;6:23508.
43) Yoshizato K, Tateno C, Utoh R. Mice with liver composed of human hepatocytes as an animal model for drug testing. Curr Drug Discov Technol 2012;9:63-76.
44) Gburek J, Konopska B, Juszczynska K, Piwowar A, Dziegiel P, Borska S, et al. Hemoglobin - a novel ligand of hepatocyte ectopic F1-ATPase. J Physiol Pharmacol 2015;66:823-830.

Author names in bold designate shared co-first authorship.

Supporting Information

Additional Supporting Information may be found at onlinelibrary.wiley.com/doi/10.1002/hep.31752/suppinfo.